Catalysis Science & Technology

Accepted Manuscript

This article can be cited before page numbers have been issued, to do this please use: L. Yang, B. McNichols, M. Davidson, B. Schweitzer, D. Gomez-Gualdron, B. G. Trewyn, A. Sellinger and M. A. Carreon, *Catal. Sci. Technol.*, 2017, DOI: 10.1039/C7CY00564D.

ROYAL SOCIETY OF CHEMISTRY

rsc.li/catalysis

View Article Online
DOI: 10.1039/C7CY00564D

Journal Name

ARTICLE

Noble metal-free catalytic decarboxylation of oleic acid to n-heptadecane on nickel-based metal-organic frameworks (MOFs)

Received 00th January 20xx,
Accepted 00th January 20xx

DOI: 10.1039/x0xx00000x

www.rsc.org/

L. Yang,[a†] B. W. McNichols,[b†] M. Davidson,[c] B. Schweitzer,[a] D. A. Gómez-Gualdrón,[a] B. G. Trewyn,[bc] A. Sellinger[*bc] and M. A. Carreon[*ac]

Nickel based metal organic frameworks (Ni-MOFs) were successfully synthesized using new conjugated carboxylic acid linkers. These conjugated carboxylic acid linkers were synthesized using mild Heck coupling that led to the incorporation of functional groups not possible by traditional synthetic methods. Control of linker size allows for porosity tuning of the crystalline network and high surface area, that, in theory, results in the increased accessibility to Ni metal centers for catalysis. The resultant crystalline Ni-MOFs displayed BET surface areas as high as ~314 m^2/g. To investigate their catalytic activity for conversion of oleic acid to liquid hydrocarbons, Ni-MOFs were grown on zeolite 5A beads that served as catalytic supports. The resultant catalysts displayed heptadecane yields as high as ~77% at mild reaction conditions, one of the highest yields for non-noble metal containing catalysts. The catalytic activity correlated to the concentration of acid sites. A slight decrease in catalytic activity was observed after catalysts recycling.

Introduction

Low-cost, readily available lipid-based biomass is an attractive feedstock for catalytic conversion into renewable alternative fuels. Recent research efforts have focused on converting triglycerides and fatty acids into linear, paraffinic hydrocarbons that can be potentially used as precursors for the production of liquid fuels, lubricants and/or other valuable petrochemicals.[1-6] Decarboxylation is an effective route for the conversion of carboxylic acids to linear, paraffinic hydrocarbons. Compared to biodiesel, alternative liquid fuels produced by catalytic decarboxylation are higher quality and more stable due to lower content or absence of oxygen.

Decarboxylation of carboxylic acids over various catalysts have received considerable attention. However, since many of the catalysts employ noble metals (Pd, Pt, Rh, Ru, Ir, Os) as the active species to attain good catalytic performance, industrial application is currently far from feasible due to limitations in cost and scale-up.[7-9] Few reports exist on non-noble metal catalysts such as nickel bimetallic sulfide phases and other metal oxides.[10-12] Non-noble metal catalysts are significantly lower cost, but have so far displayed limited catalytic performance in comparison to supported, noble metal catalysts. Another drawback of non-noble bimetallic sulfide catalysts is the sulfide contamination of resultant products. Therefore, it is important to design effective non-noble metal catalysts that display enhanced catalytic conversion of lipid-based biomass into clean alternative fuel hydrocarbon feedstock. This could be potentially achieved using metal organic frameworks (MOFs), that have emerged as a promising type of highly-tunable (chemically and topologically)[13] crystalline microporous material. MOFs combine desirable properties that make them ideal candidates for catalytic applications,[14] such as uniform microporosity, high surface area,[15] and (increasingly so) high thermal and chemical stability.[16,17] In principle, the metal cations or metal-based-clusters can act as the catalytic active species, and the ordered microporous structure can provide the pathway for guest and product molecules to diffuse with enhanced mass transfer.[18-20]

Herein, we report the synthesis of nickel based metal organic frameworks (Ni-MOFs) and their improved catalytic activity (as compared to Pd and Pt) for the decarboxylation reaction of fatty acids. The synthesized materials include previously non-synthesized MOFs employing novel carboxylic acid linkers. Nickel was chosen as the inorganic metal cation due to its promising catalytic activity for deoxygenation of fatty acids,[7] and its low cost (compared to Pd and Pt, the price of Ni is roughly 2,500X lower), that makes it appealing for decarboxylation and/or deoxygenation reactions. Supported nickel catalysts can afford reasonable yields of hydrocarbons in the catalytic deoxygenation of fatty acids even in the absence of hydrogen.[21,22] Our conjugated carboxylic acid linkers allow for new MOF structures to be prepared and tested for catalytic

[a] Department of Chemical and Biological Engineering, Colorado School of Mines, Golden, CO 80401
[b] Department of Chemistry, Colorado School of Mines, Golden, CO 80401
[c] Materials Science Program, Colorado School of Mines, Golden, CO 80401
* Corresponding authors: aselli@mines.edu; mcarreon@mines.edu
† Authors are co-first author

Electronic Supplementary Information (ESI) available: [NMR spectra (^1H, ^{13}C)] for BM65 and BM73 and ester precursors. BET area calculation details, information about Ni-MOFs in CoRE MOF database, simulated PXRDs. See DOI: 10.1039/x0xx00000x

View Article Online
DOI: 10.1039/C7CY00564D

activity. These Ni-based MOFs were grown on the surface of zeolite 5A beads to form Ni-MOF membrane/zeolite5A bead phases, which were then used as catalysts to convert oleic acid to liquid hydrocarbons.

Experimental methods

All chemicals were used as received without further purification unless noted. Dichloromethane (DCM, ACS), anhydrous tetrahydrofuran (THF, ≥99.9%), methyl acrylate (>99%), N,N-dicyclohexylmethylamine (NCy_2Me, 97%) and anhydrous magnesium sulfate ($MgSO_4$), were obtained from Sigma-Aldrich. Sodium hydroxide (NaOH, Pearl 97%) was obtained from Fisher Scientific. Bis(tri-tert-butylphosphine)palladium ($Pd[P(t\text{-}Bu)_3]_2$, 98%) was obtained from Strem Chemicals. Hydrochloric acid (HCl, ACS) was obtained from Macron Fine Chemicals. All glassware was base, acid, and water washed then oven-dried. ^1H and ^{13}C NMR spectra were obtained on a JEOL ECA 500 liquid-state NMR spectrometer and data obtained was manipulated in MestReNova NMR processor software.

Carboxylic linkers synthesis and characterization

General carboxylic acid synthesis. A Schlenk flask under argon and equipped with a magnetic stir bar was charged with the aromatic halide, methyl acrylate, N,N-dicyclohexylmethylamine, $Pd[P(t\text{-}Bu)_3]_2$ (catalyst used at 1 mol % level), and THF. The mixture was heated to 70°C for 24 h and periodically tested via TLC for reaction completion. The crude product mixture was extracted three times with DCM and acidic water (5% HCl). The organic layer was dried with $MgSO_4$, filtered, and the solvent removed using a rotary evaporator. The resultant crude product was then further purified by flash chromatography and excess was solvent removed using a rotary evaporator. The ester precursor was then converted to the corresponding acid by refluxing for 4 h in a NaOH (x10 mol equivalents) and methanol solution followed by cooling, acidification to >2 pH with HCl, then the pure acid product was collected by vacuum filtration.

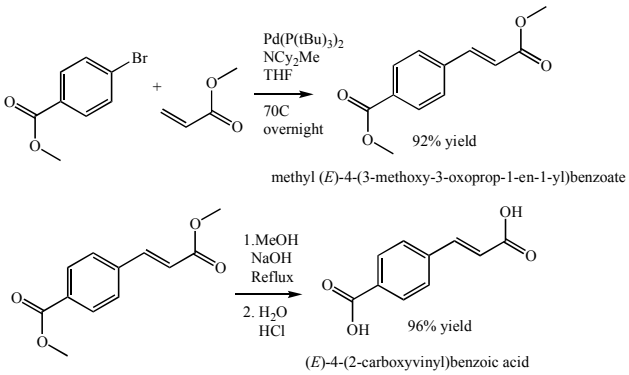

Scheme 1. Heck coupling and subsequent ester hydrolysis leading to the diacid BM 65.

BM 65 precursor (methyl (*E*)-4-(3-methoxy-3-oxoprop-1-en-1-yl) benzoate). Utilizing methyl 4-bromobenzoate (Matrix Scientific <95%) as the aromatic halide, the procedure followed the general synthesis described above, but using instead 1.1 equivalents of methyl acrylate, resulting in a white powder (92% yield) ^1H NMR (500 MHz, DMSO-d_6) δ 7.93 (s, 2H), 7.84 (s, 2H), 7.68 (d, *J* = 16.0 Hz, 1H), 6.75 (d, *J* = 16.0 Hz, 1H), 3.82 (s, 3H), 3.70 (s, 3H).

BM 65 ((*E*)-4-(2-carboxyvinyl) benzoic acid). The synthesis followed the general hydrolysis procedure described above, resulting in a white powder (96% yield) ^1H NMR (500 MHz, DMSO-d_6) δ 12.83 (s, 2H), 7.91 (d, *J* = 7.6 Hz, 2H), 7.77 (d, *J* = 7.8 Hz, 2H), 7.60 (d, *J* = 16.1 Hz, 1H), 6.61 (d, *J* = 16.2 Hz, 1H). ^{13}C NMR (126 MHz, DMSO-D_6) δ 167.83, 167.35, 143.17, 138.88, 132.34, 130.25, 128.82, 122.11

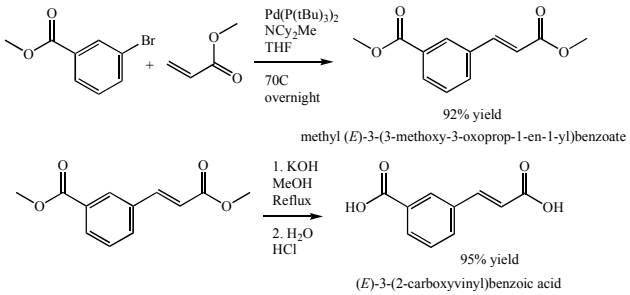

Scheme 2. Heck coupling and subsequent ester hydrolysis leading to the diacid BM 73.

BM 73 precursor (methyl (*E*)-3-(3-methoxy-3-oxoprop-1-en-1-yl) benzoate). Utilizing methyl 3-bromobenzoate (Sigma-Aldrich 98%) as the aromatic halide, followed the general synthesis above with the only change of 1.1 equivalents of methyl acrylate was utilized resulting in a white solid. (92% yield) ^1H NMR (500 MHz, DMSO-d_6) δ 8.16 (s, 1H), 7.95 (dd, *J* = 21.6, 7.8 Hz, 2H), 7.69 (d, *J* = 16.1 Hz, 1H), 7.53 (t, *J* = 7.8 Hz, 1H), 6.67 (d, *J* = 16.1 Hz, 1H), 3.83 (s, 3H), 3.69 (s, 3H). ^{13}C NMR (126 MHz, DMSO-D_6) δ 166.96, 166.30, 143.87, 135.14, 132.98, 131.28, 130.91, 129.94, 129.57, 119.76, 52.82, 52.10, 40.04.

BM 73 ((*E*)-3-(2-carboxyvinyl) benzoic acid). The synthesis followed the general hydrolysis procedure described above resulting in a white powder. (95% yield) ^1H NMR (500 MHz, DMSO-d_6) δ 8.12 (s, 1H), 7.93 (d, *J* = 4.6 Hz, 2H), 7.62 (d, *J* = 15.5 Hz, 1H), 7.51 (d, *J* = 10.8 Hz, 1H), 6.55 (d, *J* = 15.6 Hz, 1H). ^{13}C NMR (126 MHz, DMSO-D_6) δ 167.88, 167.42, 143.45, 135.20, 132.52, 132.06, 131.28, 129.80, 129.52, 120.97, 40.02.

Figures S1-S6 show the NMR spectra (1H, 13C)] for BM65 and BM73 and ester precursors.

Ni-MOF synthesis and characterization

View Article Online
DOI: 10.1039/C7CY00564D

All Ni-MOF crystals were prepared via a solvothermal approach.[23] The employed inorganic source was nickel nitrate hexahydrate (Alfa Aesar, ≥97%) and the employed organic linkers were BM 65 and BM 73, and, for comparison, the conventional BTC linker, benzene-1,3,5-tricarboxylic acid. The molar ratio of the nickel source to organic linker was kept constant at 4.08:1. In a typical synthesis, 2.0 g of nickel nitrate hexahydrate was dissolved in 15 mL of deionized water. In a separate beaker, 0.3 g of linker was dissolved in a solution mixture of 7.5 mL deionized water and 7.5 mL ethanol. The two solutions were combined and the resultant mixture was stirred thoroughly for 2 h. The mixture was transferred into a 45 mL Teflon-lined stainless steel autoclave and heated at 180 °C for 24 h. Then, the autoclave was cooled down to room temperature, and the resultant crystals at the bottom of the autoclave were washed with methanol three times. The crystals were dried overnight in the oven at 80 °C and used for subsequent characterization.

Ni-MOF/5A bead catalyst synthesis and characterization

Ni-MOF/zeolite 5A bead catalysts were prepared by solvothermally growing Ni-MOF on zeolite 5A beads (Grace Company) as described in our recent studies.[24,25] This zeolite displays LTA topology and has uniform micropores of ~0.5 nm. A similar Ni/organic linker mixture as described above was used and transferred into a 45 mL Teflon-lined stainless steel autoclave containing 5 g of pure zeolite 5A. The autoclave was then heated at 180 °C for 24 h. The resultant layered 5A beads were dried overnight at 80 °C. A second layer of Ni-MOF was applied repeating the procedure described above.

All samples were characterized by X-ray diffraction (XRD), field emission scanning electron microscopy with energy dispersive X-ray spectroscopy (FESEM-EDX), nitrogen sorption (BET), temperature programmed desorption (TPD), and thermal gravimetric analysis (TGA). XRD patterns were collected on a Kristalloflex 800 by Siemens at 25 mA and 30 kV with Cu Kα radiation. Before measurements, the Ni-MOF/zeolite 5A bead catalysts were ground by mortar and pestle into very fine powders. FESEM images were taken on JEOL ISM-7000F using a field emission gun and an accelerating voltage of 5 kV. N_2 isotherms were collected in a Micromeritics Tristar-3000 porosimeter at 77 K using liquid nitrogen as coolant. Before measurements, the samples were degassed at 180 °C for 6 h under vacuum. TPD plots were acquired on a Micrometrics Autochem 2920 instrument. Samples were pretreated under helium at 120 °C for 1 h and then up to 300 °C for 1 h. The samples were then exposed to 10 % NH_3 gas in He, followed by a temperature ramp to 100 °C to remove any physisorbed species. The samples were then ramped at 30 °C min^{-1} from 120 to 300 °C to obtain the TPD curve. Data was normalized to sample mass, and integrated using Micrometrics software suite to obtain the quantity of NH_3 adsorbed, which was equated to acid site density using a 1:1 stoichiometry. TGA profiles were obtained on a TGA Q50 under a constant flow of carbon dioxide, which is the gas atmosphere employed during the decarboxylation reactions.

Reaction procedures

Oleic acid (90%, Alfa Aesar) was used as the model fatty acid molecule. Before the reaction, the catalysts were pre-activated in an oven for 3 h at 150 °C. The reactions were conducted in a 100 mL stainless steel, high pressure batch reactor (Parr model 4560). Oleic acid and the catalyst were loaded into the reactor (mass ratio 1:1). Before the reaction was initiated, the air in the reactor was removed by flowing CO_2, followed by a pressure increase to 20 bar. Then the reactor was heated to 340 °C under constant stirring, and the temperature was kept constant during the duration of the reaction. After the reaction, the catalyst was separated from the product and washed with n-hexane 3 times, then with methanol 3 times, and finally heated at 300 °C overnight to remove the carbonaceous species formed during reaction.

Product analysis

The liquid product was collected and analyzed with a gas chromatograph (GC, 6980N) equipped with a HP-5 MS column (with dimensions of 30 m × 250 µm × 0.25 µm) and a 5973N MSD detector. Before the GC analysis, samples were silylated with N,O-bis(trimethylsilyl)trifluoroacetamide (BSTFA) (Sigma-Aldrich, ≥ 99.0%) and kept at 60 °C for 1 h. The sample (0.2 µL) was injected into the GC column (250 °C, 10.52 psi) with a 100:1 split ratio. The carrier gas was helium with a flow rate of 1.0 mL/min. The following gas chromatograph temperature program was used for the study: 100 °C for 5 min, 300 °C (1 °C/min for 2 min). The product identification was confirmed with a gas chromatograph-mass spectrometer (GC-MS).

Similar to our previous reports, the decarboxylation conversion of the oleic acid was estimated from the reduction in the number of oleic acid carboxylic acid groups during the reaction.[23-25] The amount of carboxylic acid groups remaining in the products after the reaction was evaluated by quantifying the acid number (ASTMD974). This acid number can be estimated with the mass of potassium hydroxide (KOH) in milligrams that is required to neutralize one gram of chemical substance. To quantify the acid number, a known amount of sample was dissolved in a solvent (ethanol and petroleum ether), then titrated with a solution of sodium hydroxide (NaOH, 0.1 N) using phenolphthalein as a color indicator.

The acid number was calculated from this equation:

$$\text{Acid number} = 56.1\frac{\text{NV}}{\text{W}}$$

where N=0.1 (N); V=volume of NaOH consumed (mL); W=mass of the sample (g).

The percent decarboxylation was calculated using the acid number of oleic acid and acid number of the product using the following relation: % Decarboxylation = (acid number of oleic

View Article Online
DOI: 10.1039/C7CY00564D

acid – acid number of the product) / acid number of oleic acid × 100%.

Results and Discussion

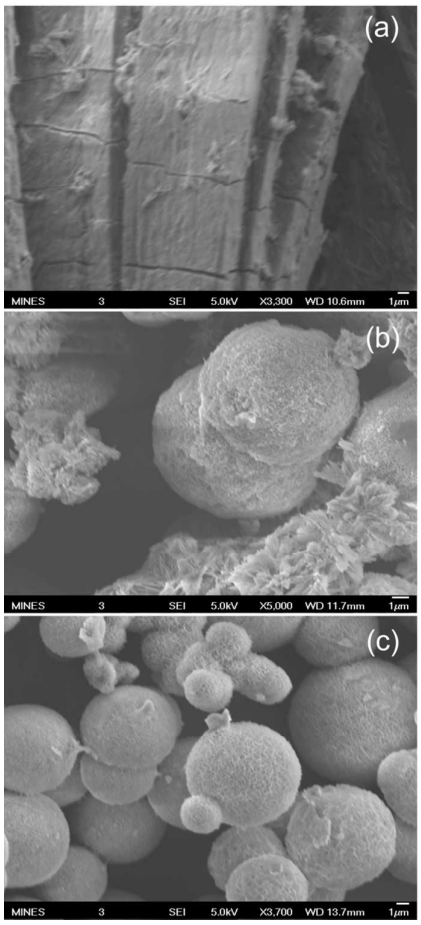

Fig. 1. Representative SEM images for Ni-MOF crystals (a) Ni-BTC MOF; (b) Ni-BM 65 MOF and (c) Ni-BM 73 MOF.

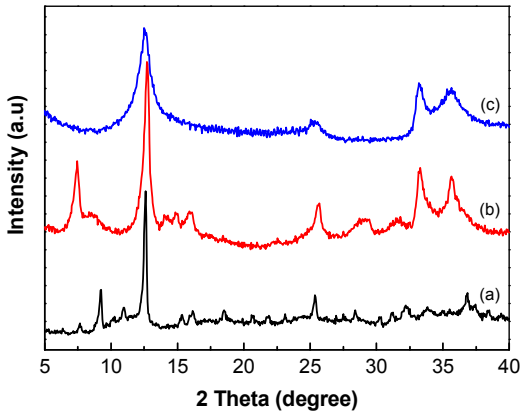

Fig. 2 XRD patterns for Ni-MOF crystals (a) Ni-BTC; (b) Ni-BM 65 and (c) Ni-BM 73.

Figure 1 shows representative SEM images of all synthesized Ni-MOF crystals. Ni-BM 65 and Ni-BM-73 crystals (Figure 1(b-c)) showed porous sphere-like structures with "raspberry" morphology, whereas Ni-BTC crystals (Figure 1(a)) showed irregular plate-like morphology with average widths of ~10 μm and lengths of varying size over 100 μm. The average size of Ni-BM 65 crystals (Figure 1(b)) was 9.0 μm. Two different particle sizes for Ni-BM 73 crystals (Figure 1(c)) were observed: 3.1 μm and 8.3 μm. To confirm the crystalline character of the synthesized materials, XRD patterns of all prepared Ni-MOFs were collected and shown in Figure 2. The materials do present crystallinity, although the varied "sharpness" of the XRD patterns for the three materials suggest varied degree of crystallinity. In particular, the relative sharpness of the patterns suggest that the larger molecule structure of the BM 65 and BM 73 linkers (as compared to BTC) led to overall lower crystallinity. PXRDs for MOFs based on these two linker present distinctive peaks at 2θ ~33° and ~36°. Although, it was not possible to experimentally solve the structure of the MOFs synthesized here to unequivocally assign the origin of these peaks, inspection of simulated XRD patterns in over 200 Ni-MOFs obtained from the computation-ready, experimental (CoRE) MOF database,[26] clearly suggest that these peaks are indicative of short range features such as Ni-Ni distances (Figure S7 presents typical arrangements of Ni atoms in CoRE MOFs).

The CoRE MOFs as a subset of structures identified as MOFs derived from the Cambridge Structural Database (CSD)[27] are a good representation of MOFs synthesized to date. By inspecting the linkers and crystallographic structures of the over 200 Ni-based CoRE MOFs (Table S1), it is clear that Ni-BM 65 and Ni-BM 73 had not been previously synthesized. The CoRE MOFs, on the other hand, revealed around 15 different Ni-MOFs that have been synthesized based on the BTC linkers. Thus, we proceeded to compare simulated XRD pattterns for these CoRE MOFs with the pattern measured here for Ni-BTC to determined whether our obtained Ni-BTC had been previously synthesized and possibly determine the crystallographic structure (Figure S7). This comparison discarded our Ni-BTC having the (3,4)-connected **tbo** topological network of the well-known Cu-BTC MOF,[28] or having a two dimensional structure. The closest match was obtained with the Ni-BTC MOF synthesized by Prior and Rosseinsky (CSD code: HUYJUG, see details in SI).[29]

The possible structures of the synthesized MOFs based on search of the CORE MOF data base [26] and *in silico* construction of MOF model using the ToBaCCo code [30] are described in the Supporting Information (Figs. S8-S14). Based on the proposed structures for Ni-BTC and Ni-BM65 (Figs. S9, and S14), a perfect crystal of these MOFs would have a pore size of 11 Å and 9 Å respectively (Figs. S11 and S16).

To confirm the porosity of the synthesized materials, the surface areas of all studied Ni-MOFs were estimated applying

View Article Online
DOI: 10.1039/C7CY00564D

BET theory to measured N_2 isotherms and listed in Table 1. To be certain of a meaningful comparison of BET areas for the synthesized is MOFs, we guided the BET area calculation with four consistency criteria as detailed in ref. 31 (see calculation details in Figures S18-S20).[31] The BET areas ranged from 12 to 303 m^2/g, with Ni-BTC presenting the lowest BET area. Given the pressumed small pore size of the three synthesized MOFs, the BET area correlates well with pore volume (Figure S23) as expected.[31] The lower observed experimental surface areas as compared to simulated surface areas may be related to the lower crystallinity of the samples and/or non optimal MOF activation conditions. The thermal stability of the synthesized MOFs was determined via TGA. As shown in Figure 3, it is confirmed that the Ni-MOF crystals are thermally stable up to (at least) 360 °C.

Table 1. BET area of studied Ni-MOFs

MOF Sample	BET area (m^2/g)	Pore volume (cm^3/g)
Ni-BTC	12	0.02
Ni-BM 65	175	0.45
Ni-BM 73	303	0.89

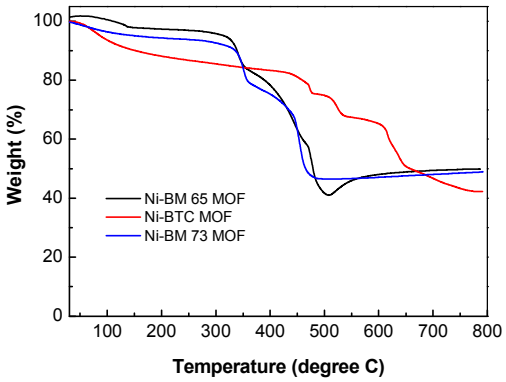

Fig. 3 TGA profiles for the studied Ni-MOF crystals.

After the described characterization of the MOFs was completed, we proceeded to grow the resultant Ni-MOFs on the surface of zeolite 5A beads, and to evaluate their catalytic ability to decarboxylate oleic acid into liquid hydrocarbons. Zeolite 5A is an aluminosilicate medium-pore-size molecular sieve with acidic sites that is commercially available at a relatively low cost. It is well known that acidic supports play an important role in the decarboxylation reaction to obtain improved heptadecane selectivities.[32,33] In addition, as compared to powders, beads are much easier to recycle and can be fully recovered, and are therefore more amenable for potential scale-up in catalytic applications.

Figure 4 shows representative SEM images of the Ni-MOF/zeolite 5A bead catalysts. The images show continuous Ni-MOF layers of 375, 538 and 415 µm thickness, respectively, for Ni-BTC, Ni-BM 65 and Ni-BM 73, respectively. XRD characterization for all catalysts showed the typical structure of zeolite 5A, which crystallizes in the LTA topology. Figures 5 (c-h) specifically confirm that the crystalline structure of zeolite 5A was preserved after Ni-MOF deposition and recycling, indicating structural stability of the 5A bead supports.

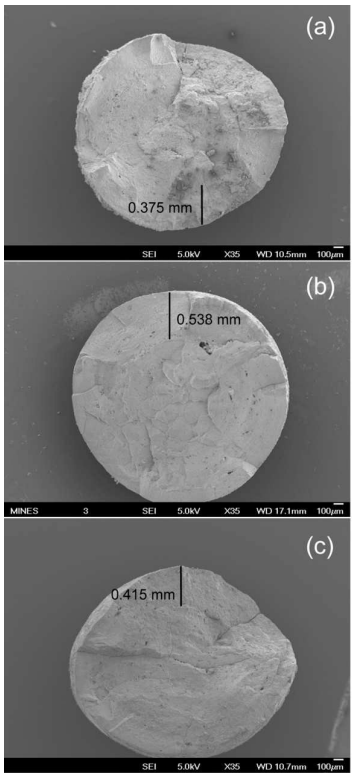

Fig. 4 SEM images for Ni-MOF/zeolite 5A bead catalysts (a) Ni-BTC MOF/zeolite 5A; (b) Ni-BM 65 MOF/zeolite 5A and (c) Ni-BM 73 MOF/zeolite 5A.

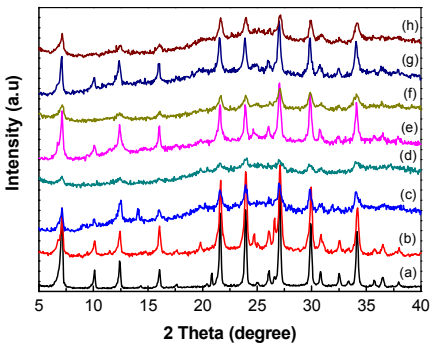

Fig. 5 XRD patterns for catalysts (a) fresh zeolite 5A; (b) spent zeolite 5A; (c) fresh Ni-BTC MOF/zeolite 5A; (d) spent Ni-BTC MOF/zeolite 5A; (e) fresh Ni-BM 65 MOF/zeolite 5A; (f) spent Ni-BM 65 MOF/zeolite 5A; (g) fresh Ni-BM 73 MOF/zeolite 5A and (h) spent Ni-BM 73 MOF/zeolite 5A.

View Article Online
DOI: 10.1039/C7CY00564D

The catalysts shown in Figure 4 were evaluated for the decarboxylation of oleic acid to liquid hydrocarbons. High conversion was observed (as high as 90% for decarboxylation) for all catalysts employed (fresh and spent) under the reaction conditions. The observed liquid product distribution for all the studied catalysts is summarized in Table 2. To clearly appreciate the role of the Ni-MOF catalysts, it is important to note that pure zeolite 5A beads provided heptadecane yields of only ~14%. Indeed, mainly short chain hydrocarbons (C_7-C_{12})

Table 2 Liquid product distribution for all studied catalysts

Catalysts	% $DeCO_x$	Hydrocarbon distribution (%)				
		Octadecane	Heptadecane	Hexadecane	Pentadecane	Tetradecane
zeolite 5A	91.3	8.18	13.91	2.12	3.56	2.75
fresh Ni-BTC MOF/zeolite 5A	91.2	1.64	70.11	2.21	3.17	0.95
spent Ni-BTC MOF/zeolite 5A	90.0	3.18	49.37	2.16	3.68	2.06
fresh Ni-BM 65 MOF/zeolite 5A	92.2	2.57	76.74	1.48	2.80	0.89
spent Ni- BM 65 MOF/zeolite 5A	90.4	1.79	56.19	1.43	3.03	1.20
fresh Ni- BM 73 MOF/zeolite 5A	90.3	2.22	71.97	1.58	2.65	1.06
spent Ni- BM 73 MOF/zeolite 5A	90.1	2.64	52.92	1.53	3.16	1.44

Catalysts	Hydrocarbon distribution (%)							
	Tridecane	Dodecane	Undecane	Decane	Nonane	Octane	Heptane	Unknown
zeolite 5A	3.84	7.43	9.16	9.90	11.36	12.91	11.79	3.06
fresh Ni-BTC MOF/zeolite 5A	1.39	2.25	2.81	2.30	4.24	4.67	3.04	1.22
spent Ni-BTC MOF/zeolite 5A	3.05	4.19	5.27	5.65	7.03	7.84	5.31	1.21
fresh Ni-BM 65 MOF/zeolite 5A	1.21	1.67	2.30	2.06	2.48	2.85	1.92	1.03
spent Ni- BM 65 MOF/zeolite 5A	1.50	2.50	3.54	4.06	7.51	9.20	6.83	1.21
fresh Ni- BM 73 MOF/zeolite 5A	1.58	2.28	3.03	2.40	3.39	4.07	2.65	1.12
spent Ni- BM 73 MOF/zeolite 5A	209	3.45	4.42	4.99	7.08	8.13	6.41	1.74

Table 3 BET areas and pore volumes for fresh and spent Ni-MOF/zeolite 5A bead catalysts

Catalysts	BET area (m^2/g)	Pore volume (cm^3/g)	Micropore volume (cm^3/g)
Zeolite 5A	549	0.28	0.220
fresh Ni-BTC MOF/zeolite 5A	188	0.20	0.032
spent Ni-BTC MOF/zeolite 5A	139	0.19	0.024
fresh Ni-BM 65 MOF/zeolite 5A	264	0.24	0.083
spent Ni- BM 65 MOF/zeolite 5A	170	0.18	0.047
fresh Ni- BM 73 MOF/zeolite 5A	164	0.15	0.050
spent Ni- BM 73 MOF/zeolite 5A	129	0.14	0.033

were observed in the presence of pure zeolite 5A beads, which are generated through cracking of oleic acid and/or long chain hydrocarbons.[34,35] Furthermore, the selectivity to heptadecane increased when zeolite 5A beads were coated with the Ni-MOFs, with the highest selectivity to n-heptadecane obtained with the Ni-BM 65/zeolite 5A catalyst. Other components in the liquid product included branched paraffins formed by isomerization of the initially formed heptadecane, and lower molecular weight hydrocarbons (mostly C_7-C_{16} paraffins) formed by cracking of the heptadecane. The observed products were: octadecane, heptadecane, dodecane, undecane, decane, nonane, octane, and heptane. A decrease

View Article Online
DOI: 10.1039/C7CY00564D

of selectivity to n-heptadecane was observed for the spent catalysts (Table 2) likely the result of surface carbon deposited on the catalysts thus lowering subsequent activity. TGA analysis indicates that indeed the amount of carbon present in the spent catalysts is higher as compared to the fresh catalysts. This observation is consistent with decreases in pore volume for all studied catalysts (Table 3) which may prevent access of oleic acid into the active sites. The Ni content of fresh and spent Ni-MOF/zeolite 5A bead catalysts were estimated by EDX. Importantly, the EDX results confirmed that there was negligible Ni leaching for all recycled spent catalysts after decarboxylation reactions (Table 4). The color of the final MOF on bead catalyst in all cases (for fresh and spent catalysts) is green, suggesting Ni^{2+} oxidation state.

Table 4 The Ni content for all studied Ni-MOF/zeolite 5A bead catalysts

Catalysts	Averaged Ni content (wt%)
fresh Ni-BTC MOF/zeolite 5A	27.49±1.46
spent Ni-BTC MOF/zeolite 5A	27.07±2.73
fresh Ni-BM 65 MOF/zeolite 5A	27.67±2.79
spent Ni- BM 65 MOF/zeolite 5A	27.23±1.55
fresh Ni- BM 73 MOF/zeolite 5A	28.21±2.94
spent Ni- BM 73 MOF/zeolite 5A	27.20±2.06

The acid sites on the as-prepared and spent MOF/zeolite 5A catalysts are summarized in Table 5. Fresh catalyst exhibited significantly higher acidity than the corresponding spent catalyst. Post-catalysis samples show approximately a 50% decrease in acid site content, except for Ni-BM 73 MOF/zeolite 5A, which shows negligible change. Ni-BM 73 also shows a reduction in the temperature of the peak desorption. The higher temperature desorption peak observed for Ni-BM73 is likely associated to free carboxylic acids of the linker that have not crystalized into the MOF framework due to the asymmetry of the linker.[36]

The desorption temperature of ammonia suggest somewhat higher Lewis acidity for Ni BTC than for Ni BM65. This is consistent with DFT-calculated charges of Ni in the nodes of the proposed structures for Ni BTC (Ni = + 0.95) and for Ni BM 65 (Ni = +0.56, + 0.73) as shown in Fig. S17

Table 5 Summary of acid site density data from TPD of NH_3 post catalysis

Catalysts	T_{max} (°C)	Acid site density (µmol/g)
zeolite 5A	255	1451
fresh Ni-BTC MOF/zeolite 5A	213	952
spent Ni-BTC MOF/zeolite 5A	206	494
fresh Ni-BM 65 MOF/zeolite 5A	205	1382
spent Ni- BM 65 MOF/zeolite 5A	196	423
fresh Ni- BM 73 MOF/zeolite 5A	300	456
spent Ni- BM 73 MOF/zeolite 5A	196	441

Table 6 Comparison of the catalytic conversion of oleic acid to heptadecane through different catalysts[a]

Entry	Catalyst	Reaction conditions	Mass ratio of metal to oleic acid	Conversion (%)	Heptadecane selectivity (%)	Ref
1	Activated carbon	T=370 °C, t=3 h	-	80±4	7±1	1
2	$Co_{0.5}Mo_{0.5}$	T=300 °C, t=3 h	1:40	88.1	6.1	5
3	5CoAl	T=330 °C, P=50 bar, LHSV=2 h^{-1}	-	100.0	47.0	9
4	5NiAl	T=330 °C, P=50 bar, LHSV=2 h^{-1}	-	93.0	25.5	9
5	Sulfide Mo/P/Al_2O_3	T=320 °C	-	81.9	76.0	10
6	Sulfide NiW/Al_2O_3	T=340 °C	-	85.7	75.5	10
7	MgO-Al_2O_3	T=400 °C	1:42	98	6.93	11
8	$Ce_{0.6}Zr_{0.4}O_2$	T=300 °C, t=6 h	1:40	94.6	11	12
9	Mo/Zeol	T=360 °C, P=20 bar, t=1 h	-	-	19	37
10	SnAlMg-2	T=300 °C, t=6 h	1:75	71.1	3.7	38
11	Ni/Al_2O_3	T=360 °C, P=20 bar, t=0.75 h	1:21505	-	10	39
12	Fe-MSN	T=290 °C, P=30 bar, t=6 h	1:4.7	100	12	40
13	NiWC/Al-SBA-15	4 h in super-critical water	1:44	97.3	5.2	41
14	Activated carbon	T=370±2 °C, P=241 bar	-	99.4±0.5	80.6±4	42
15	Mo_2N/γ-Al_2O_3	T=380 °C, P=71.5 bar, LHSV=0.45 h^{-1}	-	99.9	12	43
16	Ni/ZnO-Al_2O_3	T=280 °C, P=30 bar, t=6 h	1:100	100	95.1	44
17	Ni-BM 65 MOF/zeolite 5A	T=340 °C, P=20 bar, t=2 h	1:33	91.1	76.7	this study

[a]Only the best catalytic performance of each reference is shown in Table 6. Note: in entries 8, 9, 11, 12, 15 and 16, hydrogen is used.

View Article Online
DOI: 10.1039/C7CY00564D

Journal Name

ARTICLE

The high aptitude towards selective oleic acid decarboxylation to heptadecane of these structurally disordered MOFs does not correlate with the density of sites. The zeolite 5A support shows comparable acidity with Ni-BTC and Ni-BM 65, but minimal heptadecane yield. Therefore, Ni must play a key role in the catalytic decarboxylation of oleic acid. Interestingly, heptadecane yield scaled with micropore volume. As we move from BTC to BM 73 to BM 65 the length of the linker increases leading to progressively larger micropore volumes. Larger linkers can facilitate mass transport of the substrate and the product increasing observed yield.

We ran a reaction with a homogeneous catalyst consisting of Nickel nitrate hexahydrate and BM-65 MOF linker (reaction conditions: T=340 °C, P=20 bar, CO_2 atmosphere, t=2 h) and mass ratio of catalyst to oleic acid 1:1. The conversion was ~94%, with much lower selectivity to heptadecane (47.7%). These results suggest that indeed the presence of a MOF structure (and porosity) is needed to observe higher heptadecane selectivities (Table 6).

In addition, we evaluated the catalytic activity of Ni-BM 65 MOF powders. The Ni-MOF powders displayed good catalytic ability (~90% conversion and ~73% heptadecane selectivity). This performance was slightly lower than the Ni-BM 65 MOF/zeolite 5A (entry 17 on Table 6). We have demonstrated previously that acid supports [32,23] including 5A zeolite [24] help to improve heptadecane selectivities. Therefore, both Ni- BM 65 MOF and zeolite 5A play an important role as active sites for the decarboxylation of oleic acid to heptadecane. Further studies are needed to elucidate the specific role of each of them for this particular reaction. It is important to mention that only ~50% of the Ni-BM 65 powders were recovered after reaction, while 100% of the Ni-BM 65 MOF/zeolite 5A was recovered after reaction.

Table 6 compares the state-of-the-art non-noble metal catalysts that have been employed specifically for the catalytic conversion of oleic acid to heptadecane.[1,5,9,10-12,37-44] Sulfide Mo/P and NiW supported on Al_2O_3 had similar catalytic performance (76% selectivity to heptadecane) as Ni-BM 65 MOF/zeolite 5A bead catalyst.[10] However, the use of sulfur based catalysts may result in sulfide contamination leading to serious environmental issues. Activated carbon shows high selectivity to heptadecane 80%). However, to achieve this the pressure as high as 241 bar and temperature of 370 °C are needed.[42] Ni supported on ZnO and Al_2O_3 has displayed heptadecane selectivities higher than 95%, but the reaction requires higher pressure and longer reaction times (30 bar and 6 hours).[44] Importantly, in our study we did not employ hydrogen (we employed CO_2, a lower cost renewable feedstock), that has higher potential as a viable commercial process. The benefit of using CO_2 gas atmosphere was reported in our previous research.[25]

Conclusions

We have demonstrated the successful synthesis of nickel based metal organic frameworks (Ni-MOFs) employing novel carboxylic acid linkers. Furthermore, the deposition of these MOFs on zeolite 5A beads was illustrated and shown to produce catalytically active materials for the conversion of oleic acid into liquid hydrocarbons. The resultant Ni-MOF/zeolite 5A bead catalysts displayed heptadecane selectivity as high as ~77%. All of the studied catalysts displayed a loss in catalytic activity after recycling. This is likely due to surface carbon that deposited during the reaction, resulting in the loss of surface area and pore volume. Our efforts demonstrate that it is possible to obtain effective catalytic decarboxylation of fatty acid with non-noble metal-based catalysts. Indeed, to the best of our knowledge the catalytic performance of Ni-BM 65 MOF/zeolite 5A bead catalyst is superior to all non-noble metal state-of-the-art catalysts at *mild reaction conditions*. We also show that the use of CO_2 during reaction may lead to a more viable and cost effective route to catalytically convert fatty acid methyl esters into alternative liquid fuels. We envision the presented work will encourage synthesis and study of MOFs based on earth-abundant metals for catalytic applications.

Acknowledgements

This research was supported by the Renewable Energy Materials Research Science and Engineering Center (REMRSEC) under Award Number DMR-0820518, and by startup funds from Colorado School of Mines (CSM). B.W.M. respectfully acknowledges the sponsorship and support of the United States Air Force Institute of Technology.

References

1 J. Fu, F. Shi, L. T. Thompsom Jr., X Lu and P. E. Savage, *ACS Catal.*, 2011, **1**, 227.
2 S. De, B. Saha and R. Luque, *Bioresour. Technol.,* 2015, **178**, 108.
3 D. R. Vardon, B. K. Sharma, H. Jaramillo, DW Kim, JK Choe, P. N. Ciesielski and T. T. Strathmann, *Green Chem.,* 2014, **16**, 1507.
4 K. Hengst, M. Arend, R. Pfützenreuter and W. F. Hoelderich, *Appl. Catal., B,* 2015, **174-175**, 383.

View Article Online
DOI: 10.1039/C7CY00564D

5 JO Shim, DW Jeong, WJ Jang, KW Jeon, SH Kim, BH Jeon, HS Roh, JG Na, YK Oh, SS Han and CH Ko, *Catal. Commun.,* 2015, **67**, 16.
6 R. C. Striebich, C. E. Smart, T. S. Gunasekera, S. S. Mueller, E. M. Strobel, B. W. McNichols and O. N. Ruiz, *Int. Biodeterior. Biodefradation,* 2014, **93**, 33.
7 M. Snåre, I. Kubičková, P. Mäki-Arvela, K. Eränen and D. Y. Murzin, *Ind. Eng. Chem. Res.,* 2006, **45**, 5708.
8 A. S. Berenblyum, R. S. Shamsiev, T. A. Podoplelova and V. Y. Danyushevsky, *Russ. J. Phys. Chem. A*, 2012, **86**, 1199.
9 A. Srifa, K. Faungnawakij, V. Itthibenchapong and S. Assabumrungrat, *Chem. Eng. J,* 2015, **278**, 249.
10 T. Szarvas, Z. Eller, T. Kasza, T. Ollár, P. Tétényi and J. Hancsók, *Appl. Catal., B,* 2015, **165**, 245.
11 JG Na, BE Yi, JN Kim, KB Yi, SY Park, JH Park, JN Kim and CH Ko, *Catal. Today,* 2010, **156**, 44.
12 JO Shim, DW Jeong, WJ Jang, KW Jeon, BH Jeon, SY Cho, HS Roh, JG Na, CH Ko, YK Oh and SS Han, *Renewable Energy,* 2014, **65**, 36.
13 D. A. Gómez-Gualdrón, Y. J. Colón, X Zhang, T. C. Wang, YS Chen, J. T. Hupp, T. Yildirim, O. K. Farha, J Zhang and R. Q. Snurr, *Enery Environ. Sci.,* 2016, **9**, 3279.
14 J. Gascon, A. Corma, F. Kapteijn and F. X. Llabrés I Xamena, *ACS Catal.,* 2014, **4**, 361.
15 O. K. Farha, I. Eryazici, NC Jeong, B. G. Hauser, C. E. Wilmer, A. A. Sarjeant, R. Q. Snurr, S. T. Nguyen, A. Özgür Yazaydın and J. T. Hupp, *J. Am. Chem. Soc.,* 2012, **134**, 15016.
16 J. H. Cavka, S. Jakobsen, U. Olsbye, N. Guillou, C. Lamberti, S.Bordiga and K. P. Lillerud, *J. Am. Chem. Soc.,* 2008, **130**, 13850.
17 J. E. Mondloch, W. Bury, D. Fairen-Jimenez, S. Kwon, E. J. DeMarco, M. H. Westom, A. A. Sarjeant, S. T. Nguyen, P. C. Stair, R. Q. Snurr, O. K. Farha and J. T. Hupp, *J. Am. Chem. Soc.,* 2013, **135**, 10294.
18 K. S. Park, Z. Ni, A. P. Côté, J. Y. Choi, R. Huang, F. J. Uribe-Romo, H. K. Chae, M. O'Keeffe and O. M. Yaghi, *PNAS,* 2006, **103**, 10186.
19 G. Férey, *Chem. Soc. Rev.,* 2008, **37**, 191.
20 L. MacGillivray, *Metal Organic Framework: Design and Application,* John Wiley & Sons. Inc., 2010.
21 R. W. Gosselink, S. A. W. Hollak, SW Chang, J. van Haveren, K. P. de Jong, J. H. Bitter and D. S. van Es, *ChemsusChem,* 2013, **6**, 1576.
22 JH Wu, JJ Shi, J Fu, J.A. Leidl, ZY Hou and XY Lu, *Sci. Rep.,* 2016, DOI: 10.1038/srep27820.
23 L Yang, G. L. Ruess and M. A. Carreon, *Catal. Sci. Technol.,* 2015, **5**, 2777.
24 LQ Yang, K. L. Tate, J. B. Jasinski and M. A. Carreon, *ACS Catal.,* 2015, **5**, 6497.
25 LQ Yang and M. A. Carreon, *J. Chem. Technol. Biotechnol.,* 2017, **92**, 52.
26 Y. G. Chung, J. Camp, M. Haranczyk, B. J. Sikora, W. Bury, V. Krungleviciute, T. Yildirim, O. K. Farha, D. S. Sholl and R. Q. Snurr, *Chem. Mater.,* 2014, **26**, 6185.
27 The Cambridge Structural Database (CSD) https://www.ccdc.cam.ac.uk/
28 SS Chui, S. M. Lo, J. P Charmant, A. G. Orpen and I. D. Williams, *Science,* 1999, **283**, 1148.
29 T. J. Prior and M. J. Rosseinsky, *Inorg. Chem.,* 2003, **42**, 1564.
30 D.A.Gomez-Gualdron, Y.J.Colon, X. Zhang, T.C. Wang, Y.S. Chen, J.T. Hupp, T. Yildirim, O. K. Farha, J. Zhang, R.Q. Snurr,*Energy Environ. Sci*. 2016, 9, 3279.
31 D. A. Gómez-Gualdrón, P. Z. Moghadam, J. T. Hupp, O. K. Farha and R. Q. Snurr, *J. Am. Chem. Soc.,* 2016, **138**, 215.
32 M. Ahmadi, E. E. Macias, J. B. Jasinski, P. Ratnasamy and M. A. Carreon, *J. Mol. Catal. A: Chem.,* 2014, **386**, 14.
33 M. Ahmadi, A. Nambo, J. B. Jasinski, P. Ratnasamy and M. A. Carreon, *Catal. Sci. Technol.,* 2015, **5**, 380.
34 R. Černý, M. Kubů and D. Kubička, *Catal. Today,* 2013, **204**, 46.
35 N Ma, W. Tandar and P. E. Savage, *J. Supercrit. Fluids,* 2015, **102**, 73.
36 X Wei, YM Wang, R. Bergsträßer, S. Kundu and M. Muhler, *Appl. Surf. Sci.,* 2007, **254**, 247.
37 O. B. Ayodele, H. U. Farouk, J. Mohammed, Y. Uemura and W. M. A. W. Daud, *J Taiwan Inst Chem Eng,* 2015, **50**, 142.
38 DS Tong, CH Zhou, MY Li, MY Li, WH Yu, J. Beltramini, CX Lin and ZP Xu, *Applied Clay Science,* 2010, **48**, 569.
39 O. B. Ayodele, K. C. Lethesh, Z. Gholami and Y. Uemura, *Journal of Energy Chemistry*, 2016, **25**, 158.
40 K. Kandel, J. W. Anderegg, N. C. Nelson, U. Chaudhary and I. I. Slowing, *J. Catal.,* 2014, **314**, 142.
41 B. A. Alwan, S. O. Salley and K. Y. Simon Ng, *Appl. Catal., A,* 2015, **498**, 32.
42 S. Popov and S. Kumar, *Energy Fuels,* 2015, **29**, 3377.
43 J. Monnier, H. Sulimma, A. Dalai and G. Caravaggio, *Appl. Catal., A,* 2010, **382**, 176.
44 GC Li, F Zhang, L Chen, CH Zhang, H Huang and XB, Li, *ChemCatChem*, 2015, **7**, 2646.

View Article Online
DOI: 10.1039/C7CY00564D

Herein we demonstrate novel free-noble metal catalytic systems based on Ni MOFs that can effectively convert oleic acid into heptadecane.